mater.scichina.com link.springer.com

Published online 25 April 2024 | https://doi.org/10.1007/s40843-023-2849-6
Sci China Mater 2024, 67(5): 1533–1542

Intermolecular interaction simultaneously mediated network morphology and β-sheet crystallization of silk fibroin/polyacrylamide hydrogel for its excellent adhesive strain sensing performances

Dezhen Yang, Chuanqiang Sun, Zhe Han, Baogang Yuan, Dong Pan, Jinchuan Chen, Huajie Xu*, Chuntai Liu and Changyu Shen

ABSTRACT **Silk fibroin (SF), as a special natural polymer, is a good candidate for preparing flexible sensor due to its excellent biocompatibility, biodegradability and amphiphilic properties. However, the high and uncontrollable crystallization of SF makes it challenge to be utilized in excellent biomimetic SF hydrogel sensor. Neat SF hydrogel is brittle and not adhesive. Here, polyacrylamide (PAM) was introduced to the SF hydrogel to address this issue. Due to their strong intermolecular interaction, the network morphology of SF/PAM hydrogel was altered to non-Euclidean pore from Euclidean one. Meanwhile, its β-sheet crystallization was suppressed to nanoscale readily. These evolutions endow the SF/PAM hydrogel with not only enhanced mechanical properties but also excellent adhesion performance. Compared with that of neat PAM hydrogel, tensile strength, tensile failure strain, compressive strength (under 80% strain) and adhesion performance (on pig skin) of the SF8/PAM hydrogel are increased by 133.1%, 120.9%, 610.8% and 104.8%, respectively. Additionally, the amphiphilicity of SF could make the carbon nanotubes (CNTs) disperse well in hydrogel. CNT0.3/SF8/PAM hydrogel not only inherits but also improves the above properties. It exhibits excellent adhesive sensing performance with maximal gauge factor of 10.13, working strain range of 1000% and stability as long as over 500 cycles. The detection of six human activities was also demonstrated. This work affords a general strategy to achieve high-performance SF-based hydrogel and indicates that the SF/PAM hydrogel possesses great promise for applications in flexible wearable strain sensors.**

Keywords: silk fibroin, intermolecular interaction, network morphology, β-crystallization, adhesion, hydrogel strain sensor

INTRODUCTION

Recently, flexible strain sensors have been widely used in medical monitoring equipment, intelligent robots, and wearable sensors [1–3]. Due to their exceptional stretchability and biocompatibility, conductive hydrogels are considered as ideal candidate materials for flexible strain sensors [4–6]. Among these, researchers have been particularly interested in natural polymer hydrogels, such as silk fibroin (SF), which possesses unique mechanical properties, amphiphilicity, and biocompatibility [7–9].

Most hydrogel sensors are created by incorporating conductive materials into the three-dimensional (3D) network of hydrogels [10–12]. Attaining a uniform dispersion of conductive fillers within hydrogels is frequently a challenging task. When dispersion is non-uniform, it typically results in suboptimal conductivity and can adversely affect the mechanical properties of the hydrogels [13–16]. However, as for SF-based hydrogel, this issue is expected to be overcome. The amphiphilic properties of SF make it convenient to prepare SF hydrogels with outstanding electrical conductivity [17,18]. Nevertheless, the high and uncontrollable crystallization of SF poses a challenge in obtaining an excellent biomimetic hydrogel sensor [19]. Excessive growth of β-sheet crystals can deteriorate the properties of SF, resulting in a brittle and non-adhesive hydrogel [20]. Therefore, effectively controlling β-sheet crystallization in SF hydrogels has become a significant challenge in preparing SF hydrogels with outstanding performances.

This characteristic of SF arises from the highest thermostability of folding β-sheet conformation [21]. Two strategies have been proposed to address this issue. One approach involves a dynamic method, where decreasing SF concentration or introducing proper additives has been shown to be effective. For instance, Cao *et al.* [22] developed a humidity-induced crystallization strategy to create nano-crystalline cross-linked ion elastomers in an amorphous SF/lithium chloride solution, controlling the β-sheet crystal content of SF to around 20%. Kaplan's group [23] mixed enzyme-crosslinked SF protein with tyramine-modified SF or gelatin to prepare hybrid hydrogels with adjustable β-sheet crystallization. Another strategy is the chemical modification method, where various researches have utilized reactions like ring-opening addition reaction of epoxy to graft external molecular on SF [24]. However, these methods only partially disturb the β-sheet crystallization.

Inspired by these principles, this work introduces polyacrylamide (PAM) to the SF hydrogel. Due to their strong intermolecular interaction, the β-sheet crystallization of SF is readily suppressed to nanoscale. Additionally, the network morphology of the SF/PAM hydrogel is altered from Euclidean to non-Euclidean pore structure. These advancements not only

State Key Laboratory of Structural Analysis, Optimization and CAE Software for Industrial Equipment, National Engineering Research Center for Advanced Polymer Processing Technology, the Key Laboratory of Advanced Materials Processing & Mold of Ministry of Education, Zhengzhou University, Zhengzhou 450002, China

* Corresponding author (emails: xuhuajie@zzu.edu.cn or xhj1106@gmail.com)

enhance the mechanical properties of the SF/PAM hydrogel but also improve its adhesion performance. The underlying enhancing mechanisms are reasonably established based on intermolecular interaction, providing a general strategy for achieving high-performance SF-based hydrogel. The amphiphilicity of SF facilitates the dispersion of carbon nanotubes (CNTs) in the hydrogel. The CNT0.3/SF8/PAM hydrogel inherits and enhances the aforementioned properties, exhibiting excellent adhesive sensing performance with maximal gauge factor (GF) of 10.13, a working strain range of 1000%, and stability over 500 cycles. The detection demonstration of six human activities illustrates that the SF/PAM hydrogel holds great promise for applications in flexible wearable strain sensors.

EXPERIMENTAL SECTION

Materials

The silkworm cocoons were obtained from Tongxiang Silkworm Cocoon Farming Base in Zhejiang province, China. The monomer acrylamide (AM, 99.0%), multi-walled CNTs (⩾95%), chemical cross-linker *N*,*N*′-methylene dimethyl (acrylamide) (MBA, 97%), initiators potassium persulfate (KPS, 99.99%), lithium bromide (LiBr, ⩾99%), and PAM (M_n 2,000,000, 98%) were all purchased from Aladdin. Deionized water (18.25 MΩ at 22°C) was prepared before use. All reagents used in this study were not further purified.

Preparation of SF solution

The procedure for preparing SF solution involved dissolving Bombyx mori silk cocoon in a saturated LiBr solution. Initially, 30 g of the silk cocoons were chopped into fine pieces and immersed in 2 L boiling solution of 0.05 wt% anhydrous sodium carbonate. The solution was boiled for 30 min to facilitate the removal of sericin, after which the silk cocoons were extracted and thoroughly rinsed with deionized water at 60°C to eliminate any residual sericin from the silk fibers. This rinsing step was repeated no less than three times. The degummed silk was then dried in a vacuum oven at 60°C for 12 h, resulting in the acquisition of pure degummed silk. Following this, 10 g of the degummed silk was gradually introduced into a 100 mL solution of 9.3 M lithium bromide and allowed to dissolve in a water bath maintained at 60°C for 2 h. The silk solution was then filtered to remove any particulate impurities and subsequently dialyzed in deionized water within a dialysis bag (molecular weight cutoff: 12,000–14,000 Da) for three days. Post-dialysis, the SF solution was carefully concentrated in an ice bath until it achieved a minimum solid content of 10 wt%. The final SF solution was preserved in a refrigerator at 4°C for future applications.

Preparation of CNT0.3/SF8/PAM hydrogels and other hydrogels

Typically, 36 mg of CNTs was incorporated into a 15 mL solution containing 8 wt% SF. The mixture was subjected to magnetic stirring at 150 r min^{-1} for 20 min to ensure a homogenous dispersion of the SF/CNTs solution. Subsequently, 2.13 g of AM monomer, 10 mg of KPS, and 2 mg of MBA were precisely weighed and added to the aforementioned solution. This was followed by magnetic stirring at the same conditions (150 r min^{-1} for 20 min) to achieve a well-mixed solution. To remove any entrapped air in solution, the solution was purged with high-purity nitrogen gas and subjected to degassing using a circulating water vacuum pump for 30 min. Afterwards, 15 mL of the degassed mixture solution was transferred into a custom

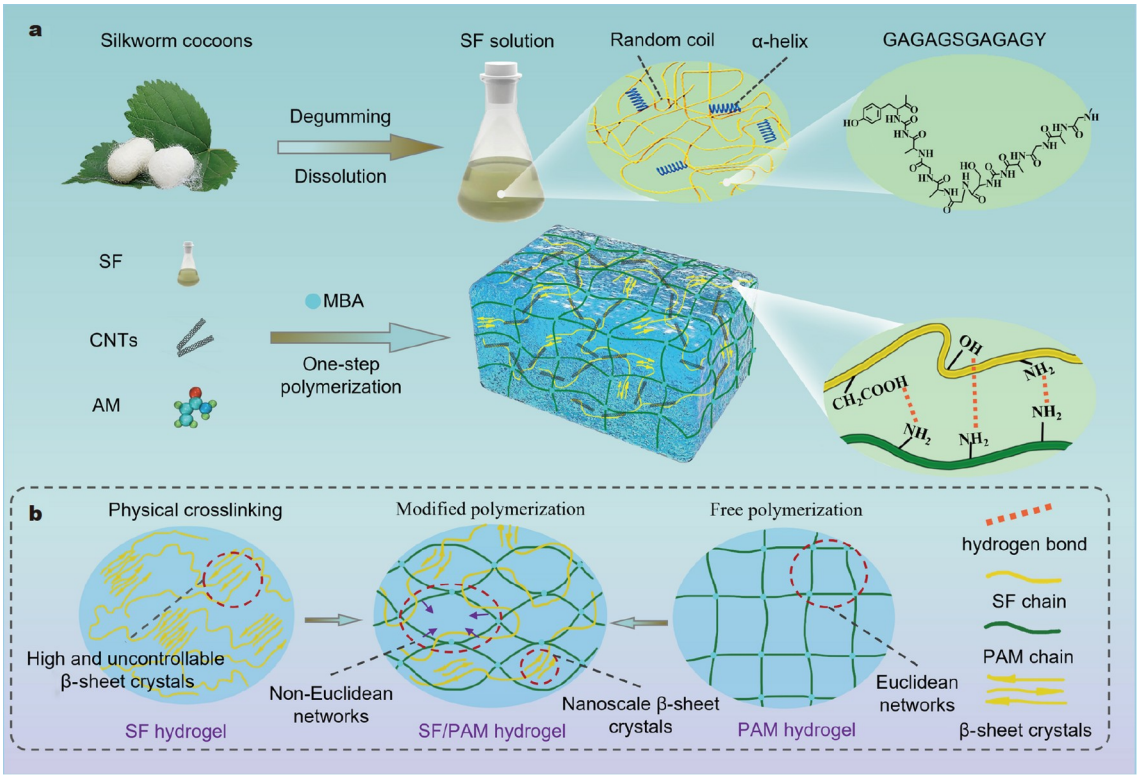

Figure 1 (a) Schematic diagram of preparation process of CNT/SF/PAM hydrogels. (b) Evolution of polymer network morphology and β-sheet crystallization simultaneously induced by strong intermolecular interaction in the SF/PAM hydrogel.

mold and cured in a convection oven at 60°C for 40 min to initiate thermal polymerization, leading to the formation of the CNT0.3/SF8/PAM hydrogel. The synthesis of other hydrogel variants followed a similar protocol. The compositional ratios of the SF/PAM and CNT/SF/PAM hydrogels are detailed in Table S1. For ease of reference, SF/PAM hydrogels with varying SF concentrations were designated as SF*x*/PAM, where *x* represents the percentage of SF. Similarly, CNT/SF/PAM hydrogels with different CNT ratios (*y*%) and SF concentrations (*x*%) were labeled as CNT*y*/SF*x*/PAM.

RESULTS AND DISCUSSION

Non-Euclidean pore and suppressed β-sheet crystallization induced by intermolecular interaction

The fabrication process of the CNT/SF/PAM hydrogel, alongside the evolution of polymer network morphology and β-sheet crystallization, is illustrated in Fig. 1. Neat SF hydrogel typically suffers from high and uncontrollable β-sheet crystallization, rendering it brittle and non-adhesive [20,25]. When PAM was introduced into SF hydrogels, strong intermolecular interaction would produce two effects. One is the suppressed β-sheet crystallization. According to reference, nano phase in polymer could improve its strength and toughness [26]. Meanwhile, strong intermolecular interaction would also alter polymerization model of PAM. As known to all, PAM is relatively hydrophobic [27]. As for neat PAM hydrogel, the free polymerization model would produce Euclidean porous networks (polygonal). However, the amphiphilic nature of SF induces a minimum free energy state in the polymer networks, transitioning from Euclidean to non-Euclidean porous networks (circular).

To verify the strong intermolecular interaction between SF and PAM, both experiment and simulation approaches were employed. Fig. 2a demonstrates a model highlighting the SF segments prone to crystallization (highly repetitive hydrophilic GAGAGY and hydrophobic GAGAGS sequences) [28,29], and the PAM chains. The interaction between SF and PAM is vividly revealed by Independent Gradient Model based on Hirshfeld partition (IGMH) analyses [30]. As shown in Fig. 2b, the presence of numerous green and blue circular flattened iso-surfaces between the polymer chains clearly indicates a strong interaction. Fig. 2c presents the relationship of δ_g^{inter} and sign(λ_2)ρ of two chains, where the colors blue, green, and red denote strong attraction, van der Waals forces, and strong repulsion, respectively. This indicates the existence of strong hydrogen bonding and van der Waals interactions between two chains. The comparative stability of neat SF aqueous solution and the SF-PAM (M_n = 2 million) mixture at room temperature (Fig. S1) further confirms the simulation findings. The SF spontaneously gelates in pure solution after standing for six days. However, it can be prolonged twice for their mixture solution.

The strong intermolecular interaction between SF and PAM significantly influences the polymer network morphology of hydrogels. Due to the absence of direct observational tools to

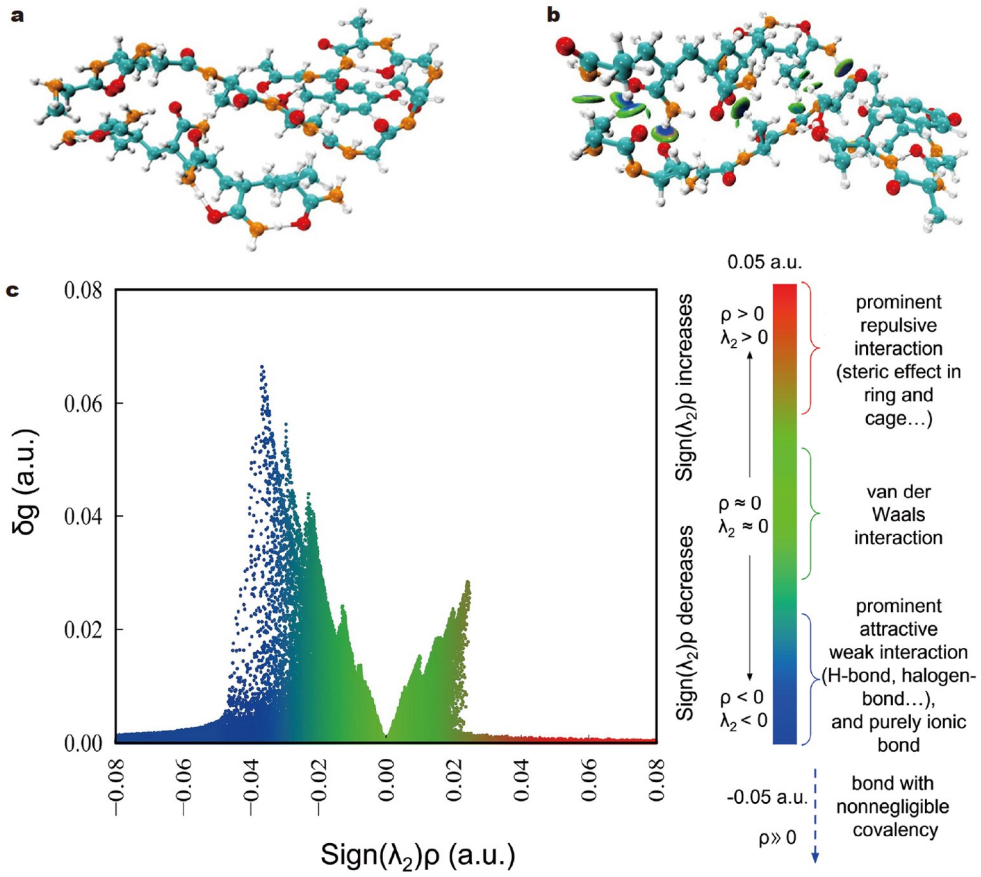

Figure 2 (a) Optimized chemical model for SF chain segment and PAM chain segment, (b) IGHM simulation of SF and PAM molecular segment, and (c) scatter map between sign(λ_2)ρ and δ_g.

characterize this effect, freeze-dried hydrogels were employed for the network morphology analysis. As shown in Fig. 3a and Fig. S2, two phenomena could be found. Neat PAM hydrogel exhibits a Euclidean pore network, while the inclusion of SF transforms into non-Euclidean one. Additionally, pore sizes are relatively uniform and decreases progressively with increasing SF concentration from 2% to 8%. At an SF concentration of 10%; however, the hydrogel exhibits some larger pores, and the distribution becomes less uniform. When CNTs were introduced into the SF/PAM hydrogel, this network morphology would be maintained. This is evident in the CNT0.3/SF8/PAM hydrogel shown in Fig. 3a. A lot of CNTs could be found in the polymer networks obviously. It confers adequate electrical conductivity to the hydrogel and affords the premise to render the hydrogel good strain sensor.

In addition to network morphology, hydrogel polymer network also plays a pivotal role in determining hydrogel properties [31]. Atomic force microscopy (AFM) was utilized to analysis the polymer network of SF/PAM hydrogels. Fig. 3b, c reveal that the modulus of the PAM aerogel polymer network is uniformly around 4 GPa, whereas the SF8/PAM aerogel polymer network comprises an 8 GPa matrix and uniform 20 GPa nanoparticles with diameter of about 30 nm. This suggests that PAM incorporation into SF results in a uniform dual polymer network, strongly indicating the presence of strong intermolecular interactions between SF and PAM. The uniform 20 GPa nanoparticles signify the formation of uniform SF β-sheet nanocrystals in the SF8/PAM hydrogel. Therefore, it can be concluded that SF8/PAM hydrogel should be a nano β-sheets crystal reinforced hydrogel with double polymers networks.

The strong intermolecular interaction between SF and PAM also mediates the β-sheet crystallization within hydrogel. The Fourier transform infrared spectroscopy (FTIR) of the SF/PAM in Fig. S3a shows prominent peaks related to amide group,

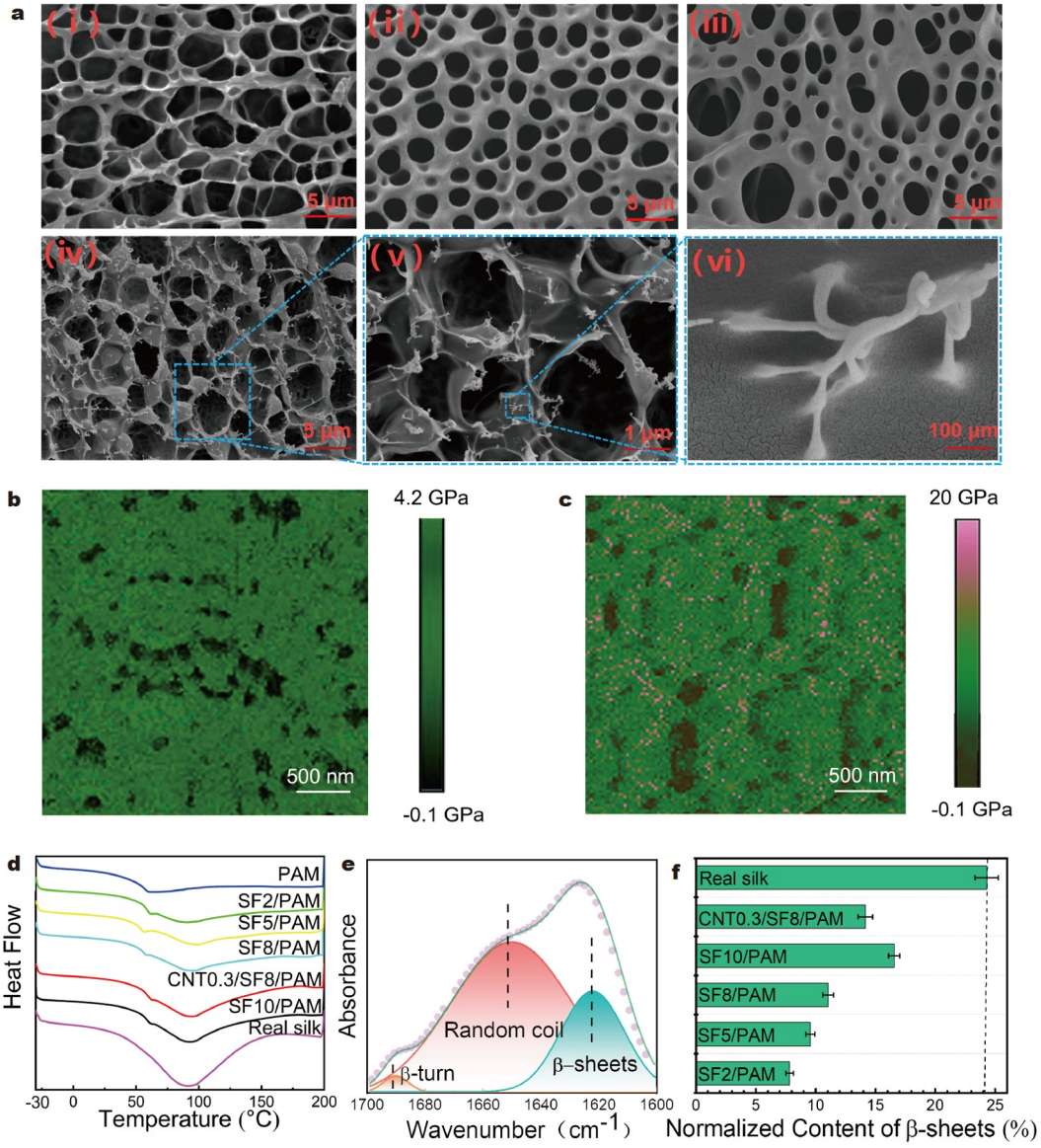

Figure 3 (a) SEM images of freeze-dried (i) neat PAM, (ii) SF8/PAM, (iii) SF10/PAM and (iv–vi) CNT0.3/SF8/PAM hydrogel. AFM modulus images of freeze-dried (b) neat PAM and (c) SF8/PAM hydrogel. (d) DSC curves of six kinds of hydrogels and real silk. (e) Deconvolution of FTIR spectra for real silk. (f) Normalized β-sheets crystallization of five kinds of hydrogels and real silk.

including amide I (1640 cm^{-1}), amide II (1515 cm^{-1}), and amide III (1235 cm^{-1}) [32]. However, it is difficult to distinguish SF and PAM due to the overlap of their amide peaks. Fig. S3b shows the wide-angle X-ray diffraction (WAXD) patterns of SF/PAM hydrogels. It can be seen that diffraction peaks can be observed at 20.5°, indicating the presence of typical silk II structure, i.e., β-sheets crystalline phase [33]. Quantitative analysis of these alterations was performed using differential scanning calorimetry (DSC) on the corresponding aerogels. Neat PAM exhibits a small exothermic peak around 55°C, while primitive SF fiber exhibits one around 95°C in Fig. 3d. The β-sheet content of primitive SF fiber was determined by deconvoluting its infrared spectrum, allowing for the estimation of β-sheet content in each aerogel using primitive SF fibers as a reference. Fig. 3e, f demonstrate that the normalized crystallization degree of the SF/PAM aerogel is significantly reduced compared with that of primitive SF fiber. For SF8/PAM aerogel, the crystallization degree is reduced to 12%. Moreover, although CNTs may promote SF crystallization, the crystallization degree of the CNT0.3/SF8/PAM hydrogel does not exceed 15%. Given crystallization propensity of SF, these values suggest that the hydrogels would have a lower crystallization degree than their corresponding aerogels. It can be concluded that the introduction of PAM in SF hydrogel would suppress β-sheets crystallization.

Enhanced mechanical properties and emerging adhesion performance

The presence of nano β-sheets and non-Euclidean polymer networks serves to enhance the strength and toughness of hydrogel. As nanocrystals are minute nanoparticles, they likely facilitate lubrication within the SF/PAM hydrogels, allowing them to move with the polymer chains during stretching and enabling a broad range of flexible polymer chain movements [26,34]. Thus, the inhibited β-sheet crystallization is advantageous to these mechanical properties. To qualitatively demonstrate the effect of non-Euclidean polymer networks on the strengthening and toughing of the SF/PAM hydrogel, three typical 2D representative volume element (RVE) models with identical pore area were simulated by COMSOL Multiphysics software (Fig. S4). Fig. 4a reveals that under 800% strain, the hexagonal pore model exhibits significant stress concentration compared with the circular pore model, with smaller circular pores showing less stress concentration than larger ones. These findings are supported by calculations based on real RVE models extracted from scanning electron microscopy (SEM) images of neat PAM and SF8/PAM hydrogels, as seen in Fig. S5. Therefore, it is clear that the non-Euclidean network morphology induced by intermolecular interaction would make SF/PAM hydrogels stronger and tougher.

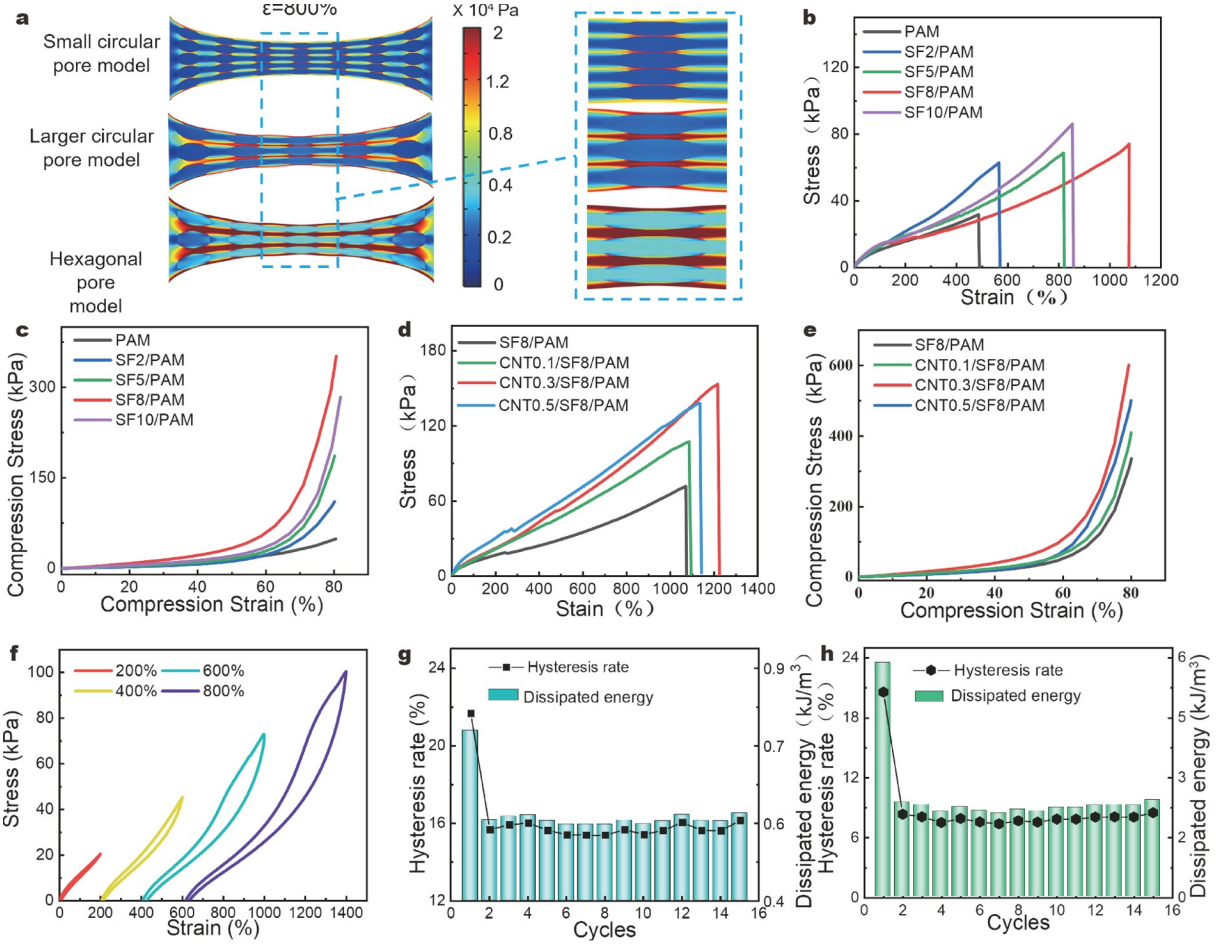

Figure 4 (a) Stress distribution of hydrogels with different typical network morphologies calculated by COMSOL. (b) Tensile and (c) compressive stress-strain curves of SF/PAM hydrogels. (d) Tensile and (e) compressive stress-strain curves of CNT/SF8/PAM hydrogels. (f) Continuous cyclic tensile strain curves of CNT0.3/SF8/PAM hydrogel at different strains (shifted along strain axis for clarity). Dissipated energy and energy dissipation rate of CNT0.3/SF8/PAM hydrogel under loading-unloading cycles at (g) 200% tensile strain and at (h) 80% compressive strain for 15 cycles.

Fig. 4b, c show that the mechanical properties of SF/PAM hydrogels surpass those of neat PAM hydrogel. As the SF concentration increases from 0 to 8%, the tensile stress of the SF/PAM hydrogels increases from 31.8 ± 4.3 to 87.1 ± 7.1 kPa, and the compression strength escalates from 49.1 ± 6.2 to 335.9 ± 9.4 kPa. Meanwhile, the tensile failure strain extends from 486.9% ± 4% to 1076.1% ± 24%. At an SF concentration of 10%, the tensile strength peaks, but the tensile failure strain diminishes relative to the SF8/PAM hydrogel, due to the formation of larger β-sheet crystals that reduce the toughening effect [35]. The viscoelastic properties in Fig. S6 show similar tendency.

The hydrogel prepared with 8% SF concentration features a uniform small non-Euclidean network and nano β-sheet reinforcement, resulting in the most optimal mechanical properties. To leverage this advantage, CNTs were exclusively introduced into this hydrogel. Fig. 4d, e show the addition of a small amount of CNTs further enhances the tensile and compressive properties, likely due to the maintained non-Euclidean network and the physical entanglement between the rigid CNTs and the SF molecular chains. The CNT0.3/SF8/PAM hydrogel demonstrates superior tensile and compressive properties. Fig. 4f exhibits continuous stretching and relaxation curves of this hydrogels at various strains. Below 400% strain, the hydrogel exhibits almost no hysteresis, with the curves nearly overlapping. Notable hysteresis is observed only at strains above 400%. This phenomenon is mainly dominated by its polymer networks. At low strain, the deformations are primarily accommodated by flexible PAM chains, which quickly revert upon tension release. At high strain, the rigid SF chains also start to deform and move in the hydrogel network, causing a hysteresis effect after unloading [36]. Fig. 4g, h and Fig. S7 display the energy dissipation of the hydrogel under 200% tensile strain and 80% compressive strain, revealing significantly higher dissipative energy of 5.82 and 0.76 kJ m^{-3} in the first tensile and compressive cycle. In subsequent cycles, the tensile and compressive dissipative energies stabilize at 2.91 and 0.65 kJ m^{-3}, respectively, indicating excellent resilience and shape recovery performance. The hysteresis rate follows the same pattern as energy dissipation. Additionally, Fig. S8 indicates the hydrogel has reached the

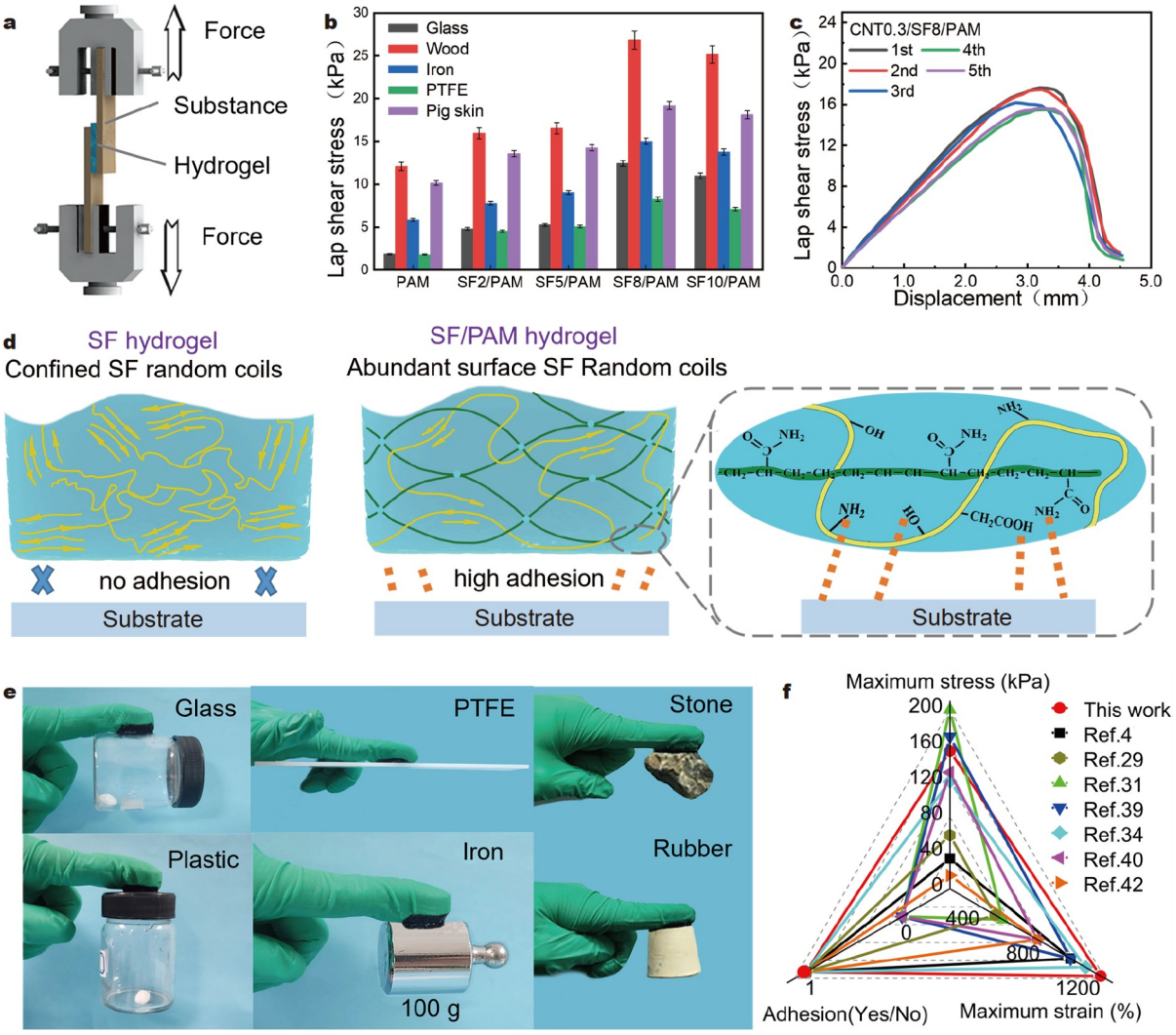

Figure 5 (a) Schematic illustration of hydrogel lap shear test device. (b) Adhesion strength of SF/PAM hydrogels with different SF contents on different substrates (glass, wood, iron, polytetrafluoroethylene (PTFE), and pigskin). (c) Cyclic adhesion strength of the CNT0.3/SF8/PAM hydrogel on pig skin. (d) Adhesion mechanism of SF/PAM hydrogel. (e) Photos of the CNT0.3/SF8/PAM hydrogel adhesions on different substrates. (f) Comparison of mechanical properties of the CNT0.3/SF8/PAM hydrogel with other recent references.

percolation threshold for electrical conductivity. Consequently, the CNT0.3/SF8/PAM hydrogel is selected as a promising candidate for flexible strain sensor.

The criticality of adhesion performance for wearable strain sensors is well-documented [37,38]. The evaluation of the hydrogel adhesion was conducted using a lap shear device depicted in Fig. 5a. Fig. 5b and Fig. S9 illustrate the lap shear stress and curve for five different hydrogels on various substrates, respectively. Overall, the inclusion of SF markedly enhances the adhesion performance of all hydrogels. Notably, the SF8/PAM hydrogel demonstrates the highest adhesion across all tested substrates, with instantaneous adhesion strengths measured at 13.2 ± 0.52 kPa on glass, 27.4 ± 1.37 kPa on wood, 15.8 ± 0.38 kPa on iron plate, 8.8 ± 0.35 kPa on polytetrafluoroethylene, and 20.1 ± 0.8 kPa on pigskin. In particular, the lap shear stresses of hydrogels on wood and pigskin exhibit significantly higher values compared with other substrates. Fig. 5c reveals that the CNT0.3/SF8/PAM hydrogel maintains similar lap shear stress to the SF8/PAM hydrogel, preserving over 92% of its strength. Additionally, the cyclic peel-off adhesive test on CNT0.3/SF8/PAM hydrogels indicates that approximately 80% of the original adhesion strength is retained after five cycles.

The robust adhesion of SF/PAM hydrogels to a variety of substrates is attributed to the presence of amino, carboxyl, and hydroxyl groups in the hydrogel, facilitating diverse and significant interfacial interactions. However, the neat SF hydrogel lacks adhesion properties. The suppression of β-sheet crystallization enhances the adhesion capabilities of SF-based hydrogels. This mechanism based on the inhibition of β-sheet crystallization is illustrated in Fig. 5d. β-sheet crystalline phases are inherently hydrophobic. For the neat SF hydrogel, the extensive and uncontrolled β-sheet crystallization confines numerous SF random coils within the hydrogel matrix. Conversely, the strong intermolecular interaction between SF and PAM inhibits β-sheet crystallization, allowing a sufficient amount of SF random coils to be exposed on the hydrogel surface, thereby improving adhesion performance. As for SF10/PAM hydrogel, with a higher concentration of SF, diminishes the impact of intermolecular interactions, leading to increased β-sheet crystallization and a consequent reduction in adhesion performance. Direct evidence supporting this adhesion perfor-

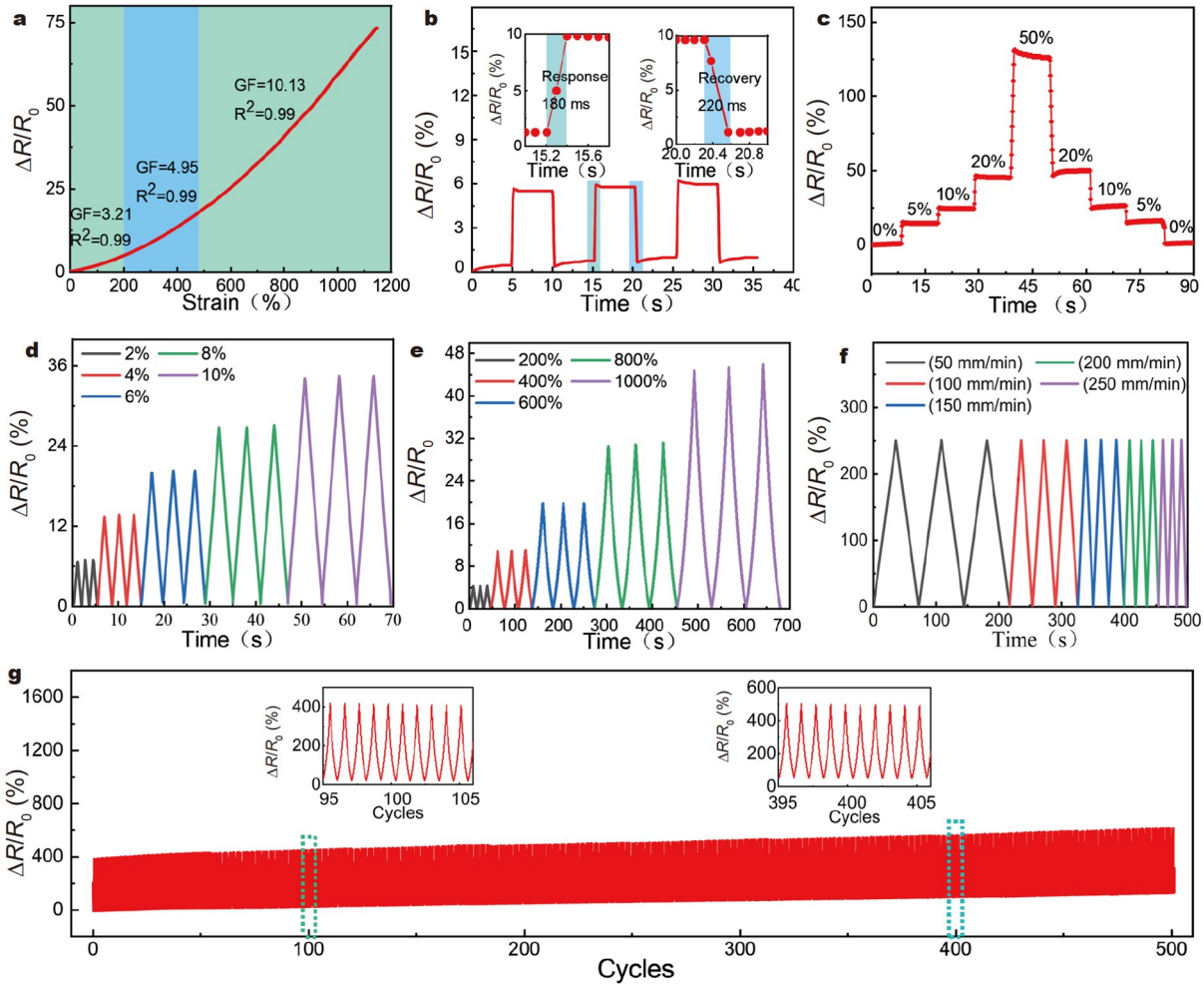

Figure 6 (a) Relative resistance variation and GFs of the CNT0.3/SF8/PAM hydrogel in the wide working ranges. (b) Response time and recovery time of the CNT0.3/SF8/PAM hydrogel at 1% tensile strain. (c) Relative resistance variation curve of the CNT0.3/SF8/PAM hydrogel under 0–50% tensile strains. Relative resistance variation of the CNT0.3/SF8/PAM hydrogel under (d) small (2%–10%) and (e) large (200%–1000%) tensile strains. (f) Relative resistance variation of the CNT0.3/SF8/PAM hydrogel when stretched to 200% at different strain rates. (g) Relative resistance variation of the CNT0.3/SF8/PAM hydrogel under 500 tensile cycles at 200% strain.

mance is presented in Fig. 5e. Overall, as shown in Fig. 5f, the CNT0.3/SF8/PAM hydrogel outperforms most reported hydrogels [39]. Moreover, it exhibits exceptional puncture resistance as depicted in Fig. S10.

Excellent sensing performance of the CNT0.3/SF8/PAM hydrogel

The strain sensing capabilities of the CNT0.3/SF8/PAM hydrogel were thoroughly assessed in Fig. 6. As compared in Table S3, it exhibits outstanding stretchability, ultrafast response, high strain sensitivity and excellent electrical stability. The hydrogel sensors hold GFs of 3.21, 4.95, and 10.13 in the strain ranges of 0–200%, 200%–450%, and 450%–1180%, respectively. These GFs surpass those of most hydrogel strain sensors reported in literature, indicating that this sensor possesses high sensitivity over a wider range of strain [40]. The three distinct GF regions can be attributed to the transformation of contact resistance effect and the tunneling effect [41]. At strains of 0–200%, CNTs dispersed in the hydrogel still contact with each other. GF is dictated by its geometric alteration. Thus, it is a small value. Strain of 200%–450% is a transition range between the tunneling resistance and contact resistance. This GF is a moderate one. Beyond 450% strain, CNTs may slide and even break apart. It significantly disrupts the conduction path and causes a sharp decrease in electric conductivity. Thus, this region has the highest GF.

The response rate of the CNT0.3/SF8/PAM hydrogel was gauged through instantaneous stretching and releasing at a tensile strain of 2%. As shown in Fig. 6b, the hydrogel response is instantaneous, with the response and recovery times for stretching and relaxation clocking in at 180 and 220 ms, respectively, when the sensing signals are amplified. This difference is consistent with its cyclic mechanical properties. Fig. 4g, h show some hysteresis still exists no matter cyclic tensile or compressive loading. As for unloading process, the recombination of hydrogen bonds in the hydrogel takes a certain amount of time. Thus, it needs a slightly longer recovery time than the response time. This minor delay is negligible in comparison to the duration of the stretch-release cycle. At the same time, Fig. 6c exhibits the hydrogel maintains stable $\Delta R/R_0$ signals under steady strain. To evaluate its stability, sensing tests were conducted under various strain and loading rates. Fig. 6d–f confirm that reliable $\Delta R/R_0$ signals are consistently obtained under all tested conditions. Stability and durability are paramount for strain sensor applications [42]. Fig. 6g illustrates that $\Delta R/R_0$ remains consistent over 500 cyclic stretches and releases at 200% strain. This outstanding repeatability with negligible fluctuations indicates that the CNT0.3/SF8/PAM hydrogel sensor possesses good anti-fatigue properties and can be used for a long time.

Human activity monitoring of the CNT0.3/SF8/PAM hydrogel

Due to its superior mechanical properties, significant adhesion and excellent sensing capabilities, the CNT0.3/SF8/PAM hydrogel can be applied as electronic skin for detecting various activities of human body. After directly adhering it to different parts of the body, a wide range of human activities can be detected in real time. Fig. S11 exhibits the size of the prepared hydrogel sensor device is 20 mm × 10 mm × 1.5 mm. As shown in Fig. 7a, the relative resistance signal $\Delta R/R_0$ increases

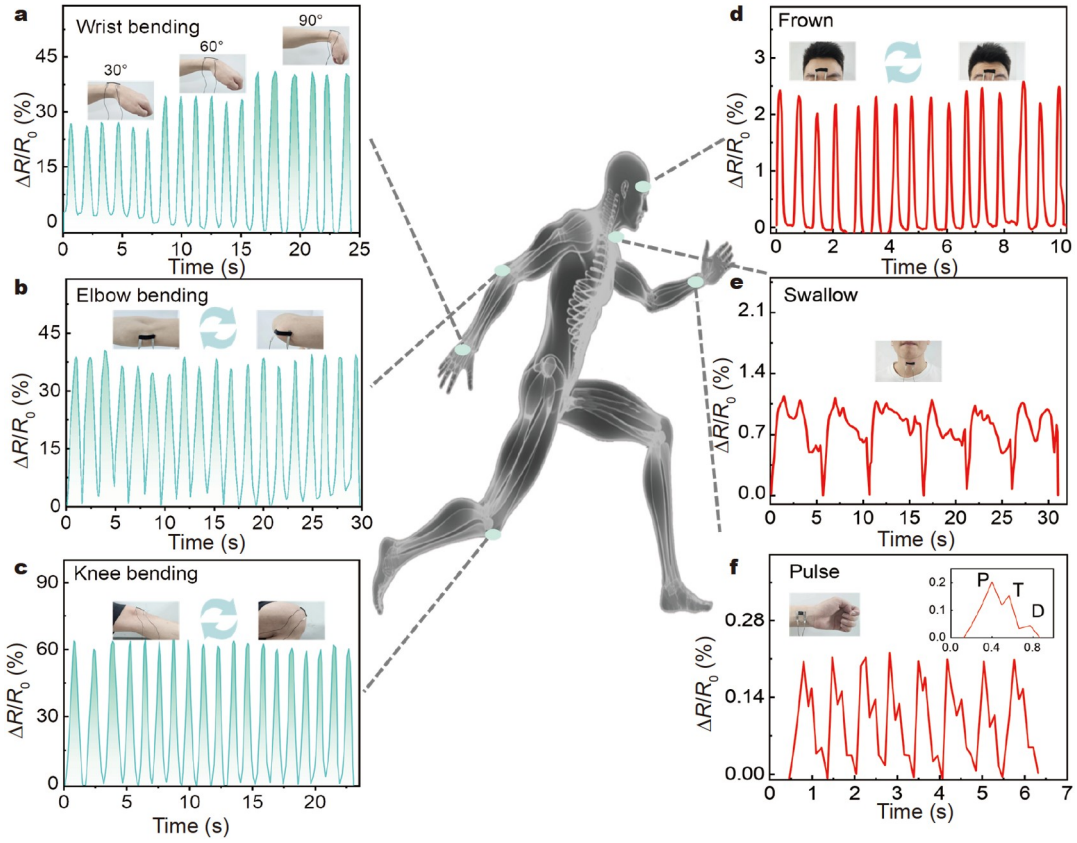

Figure 7 Real-time relative resistance changes of CNT0.3/SF8/PAM sensors for monitoring the following human activities: (a) repeated wrist flexion at different angles, (b) repeated elbow flexion, (c) repeated knee flexion, (d) repeated frowning, (e) repeated swallowing, and (f) human pulse at rest.

correspondingly as the wrist bending angle increases from 30° to 90°. Furthermore, the signals can instantly return to its initial state when the elbow is extended and stable at the same angles. Similarly, Fig. 7b, c show the bending movements of the elbow and knee can also be accurately detected in real time using the CNT0.3/SF8/PAM hydrogel electronic skin. In addition, as a multi-purpose electronic skin, the CNT0.3/SF8/PAM hydrogel can not only respond to large joint movements of the human body but also accurately identify and monitor subtle movements, including frowning, swallowing, and pulsation. When the hydrogel is fixed on the volunteer's forehead, high-frequency frowning signals can be detected (Fig. 7d). When it is fixed on the throat, the corresponding $\Delta R/R_0$ electrical signal changes rapidly, allowing clearly distinguishing of deformations during the swallowing process (Fig. 7e). Importantly, as exhibited in Fig. 7f, the wrist-attached electronic skin can detect pulse rate under slight pressure conditions and every single pulse peak in relaxation clearly distinguishes the characteristics of the pulse waveform, namely "P" (percussion), "T" (tidal), and "D" (dicrotic) [43]. These applications obviously demonstrate the high sensitivity of the CNT0.3/SF8/PAM hydrogel in discerning subtle human movements. It shows SF/PAM hydrogels possess great promise for applications in flexible wearable strain sensors.

CONCLUSIONS

Herein, the introduction of PAM into SF networks has been explored to simultaneously modulate the network morphology and β-sheet crystallization. The strong intermolecular interaction between SF and PAM molecular chain is confirmed by both experiment and density functional theory simulation. This modification transforms the network morphology from Euclidean to non-Euclidean pores and delicately suppresses β-sheet crystallization to the nanoscale. These advancements significantly enhance the mechanical properties and adhesion performance of the SF8/PAM hydrogel. The effects of network morphology on hydrogel strengthening and toughening are evaluated emphatically. Compared with neat PAM hydrogel, its tensile strength, tensile failure strain, compressive strength (under 80% strain) and adhesion performance (on pigskin) increase by 133.1%, 120.9%, 610.8%, and 104.8%, respectively. Additionally, the amphiphilicity of SF could make CNTs disperse well in hydrogel. The CNT0.3/SF8/PAM hydrogel further improves the properties. It exhibits excellent adhesive sensing performance with a maximal GF of 10.13, a working strain range up to 1000%, and stability over 500 cycles. The detection of six human activities is also demonstrated. In a word, this work affords a general strategy to achieve high-performance SF-based hydrogel which exhibits great potential in the applications of flexible wearable strain sensors.

Received 29 December 2023; accepted 1 March 2024; published online 25 April 2024

1 Meng K, Xiao X, Wei W, *et al.* Wearable pressure sensors for pulse wave monitoring. Adv Mater, 2022, 34: 2109357
2 Guo Y, Li H, Li Y, *et al.* Wearable hybrid device capable of interactive perception with pressure sensing and visualization. Adv Funct Mater, 2022, 32: 2203585
3 Niu H, Li H, Gao S, *et al.* Perception-to-cognition tactile sensing based on artificial-intelligence-motivated human full-skin bionic electronic skin. Adv Mater, 2022, 34: 2202622
4 Ge G, Lu Y, Qu X, *et al.* Muscle-inspired self-healing hydrogels for strain and temperature sensor. ACS Nano, 2020, 14: 218–228
5 Zhu T, Ni Y, Biesold GM, *et al.* Recent advances in conductive hydrogels: Classifications, properties, and applications. Chem Soc Rev, 2023, 52: 473–509
6 Wu F, Lin X, Xu Y, *et al.* Light-driven locomotive soft actuator and multi-functional sensors based on asymmetric PVA/carbon/PE bilayer film. Sci China Mater, 2023, 66: 4782–4793
7 Wang L, Chen Z, Yan Y, *et al.* Fabrication of injectable hydrogels from silk fibroin and angiogenic peptides for vascular growth and tissue regeneration. Chem Eng J, 2021, 418: 129308
8 Shi C, Hu F, Wu R, *et al.* New silk road: From mesoscopic reconstruction/functionalization to flexible meso-electronics/photonics based on cocoon silk materials. Adv Mater, 2021, 33: 2005910
9 Zhang Y, Sheng R, Chen J, *et al.* Silk fibroin and sericin differentially potentiate the paracrine and regenerative functions of stem cells through multiomics analysis. Adv Mater, 2023, 35: 2210517
10 Shen J, Du P, Zhou B, *et al.* An anti-freezing biomineral hydrogel of high strain sensitivity for artificial skin applications. Nano Res, 2022, 15: 6655–6661
11 Zhu J, Tao J, Yan W, *et al.* Pathways toward wearable and high-performance sensors based on hydrogels: Toughening networks and conductive networks. Natl Sci Rev, 2023, 10: nwad180
12 Wu S, Wang B, Chen D, *et al.* Highly sensitive and self-healing conductive hydrogels fabricated from cationic cellulose nanofiber-dispersed liquid metal for strain sensors. Sci China Mater, 2023, 66: 1923–1933
13 Qin Z, Sun X, Yu Q, *et al.* Carbon nanotubes/hydrophobically associated hydrogels as ultrastretchable, highly sensitive, stable strain, and pressure sensors. ACS Appl Mater Interfaces, 2020, 12: 4944–4953
14 Tropp J, Collins CP, Xie X, *et al.* Conducting polymer nanoparticles with intrinsic aqueous dispersibility for conductive hydrogels. Adv Mater, 2024, 36: 2306691
15 Ye Y, Jiang F. Highly stretchable, durable, and transient conductive hydrogel for multi-functional sensor and signal transmission applications. Nano Energy, 2022, 99: 107374
16 Wang Q, Ling S, Liang X, *et al.* Self-healable multifunctional electronic tattoos based on silk and graphene. Adv Funct Mater, 2019, 29: 1808695
17 Wang C, Xia K, Zhang Y, *et al.* Silk-based advanced materials for soft electronics. Acc Chem Res, 2019, 52: 2916–2927
18 Liang X, Li H, Dou J, *et al.* Stable and biocompatible carbon nanotube ink mediated by silk protein for printed electronics. Adv Mater, 2020, 32: 2000165
19 Yang S, Zhao C, Yang Y, *et al.* The fractal network structure of silk fibroin molecules and its effect on spinning of silkworm silk. ACS Nano, 2023, 17: 7662–7673
20 Zhao W, Gan D, Qu X, *et al.* Bioinspired wet-resistant organogel for highly sensitive mechanical perception. Sci China Mater, 2022, 65: 2262–2273
21 Tavsanli B, Okay O. Mechanically robust and stretchable silk/hyaluronic acid hydrogels. Carbohydrate Polyms, 2019, 208: 413–420
22 Cao L, Ye C, Zhang H, *et al.* An artificial motion and tactile receptor constructed by hyperelastic double physically cross-linked silk fibroin ionoelastomer. Adv Funct Mater, 2023, 33: 2301404
23 Hasturk O, Jordan KE, Choi J, *et al.* Enzymatically crosslinked silk and silk-gelatin hydrogels with tunable gelation kinetics, mechanical properties and bioactivity for cell culture and encapsulation. Biomaterials, 2020, 232: 119720
24 Sahoo JK, Hasturk O, Falcucci T, *et al.* Silk chemistry and biomedical material designs. Nat Rev Chem, 2023, 7: 302–318
25 Chang H, Meng L, Shao C, *et al.* Physically cross-linked silk hydrogels with high solid content and excellent mechanical properties *via* a reverse dialysis concentrated procedure. ACS Sustain Chem Eng, 2019, 7: 13324–13332
26 Zhu Z, Ling S, Yeo J, *et al.* High-strength, durable all-silk fibroin hydrogels with versatile processability toward multifunctional applications. Adv Funct Mater, 2018, 28: 1704757
27 Li G, Li C, Li G, *et al.* Development of conductive hydrogels for fabricating flexible strain sensors. Small, 2022, 18: 2101518
28 Wang W, Liu Y, Wang S, *et al.* Physically cross-linked silk fibroin-based

tough hydrogel electrolyte with exceptional water retention and freezing tolerance. ACS Appl Mater Interfaces, 2020, 12: 25353–25362
29 Wang J, Zhang N, Tan Y, *et al.* Sweat-resistant silk fibroin-based double network hydrogel adhesives. ACS Appl Mater Interfaces, 2022, 14: 21945–21953
30 Lu T, Chen Q. Independent gradient model based on Hirshfeld partition: A new method for visual study of interactions in chemical systems. J Comput Chem, 2022, 43: 539–555
31 Ming X, Sheng Y, Yao L, *et al.* Anti-swelling conductive polyampholyte hydrogels *via* ionic complexations for underwater motion sensors and dynamic information storage. Chem Eng J, 2023, 463: 142439
32 Kadumudi FB, Hasany M, Pierchala MK, *et al.* The manufacture of unbreakable bionics *via* multifunctional and self-healing silk-graphene hydrogels. Adv Mater, 2021, 33: 2100047
33 Yan S, Wang Q, Tariq Z, *et al.* Facile preparation of bioactive silk fibroin/hyaluronic acid hydrogels. Int J Biol Macromolecules, 2018, 118: 775–782
34 Han S, Tan H, Wei J, *et al.* Surface modification of super arborized silica for flexible and wearable ultrafast-response strain sensors with low hysteresis. Adv Sci, 2023, 10: 2301713
35 Su D, Yao M, Liu J, *et al.* Enhancing mechanical properties of silk fibroin hydrogel through restricting the growth of β-sheet domains. ACS Appl Mater Interfaces, 2017, 9: 17489–17498
36 Wang S, Yu L, Wang S, *et al.* Strong, tough, ionic conductive, and freezing-tolerant all-natural hydrogel enabled by cellulose-bentonite coordination interactions. Nat Commun, 2022, 13: 3408
37 Zheng H, Chen M, Sun Y, *et al.* Self-healing, wet-adhesion silk fibroin conductive hydrogel as a wearable strain sensor for underwater applications. Chem Eng J, 2022, 446: 136931
38 Lei B, Cao L, Qu X, *et al.* Thermal-sensitive ionogel with NIR-light controlled adhesion for ultrasoft strain sensor. Nano Res, 2023, 16: 5464–5472
39 Zhang R, Liu C, Wei C, *et al.* Thermoplastic charge-transfer hydrogels for highly sensitive strain and temperature sensors. J Mater Chem A, 2023, 11: 8320–8329
40 Wang Q, Ding H, Hu X, *et al.* A dual-trigger-mode ionic hydrogel sensor for contact or contactless motion recognition. Mater Horiz, 2020, 7: 2673–2682
41 Amjadi M, Kyung K, Park I, *et al.* Stretchable, skin-mountable, and wearable strain sensors and their potential applications: A review. Adv Funct Mater, 2016, 26: 1678–1698
42 Li Y, Yang D, Wu Z, *et al.* Self-adhesive, self-healing, biocompatible and conductive polyacrylamide nanocomposite hydrogels for reliable strain and pressure sensors. Nano Energy, 2023, 109: 108324
43 Liu Y, Xia M, Zhou Y, *et al.* Rational design of bioinspired gradient conductivity and stiffness for tactile sensors with high sensitivity and large linear range. Compos Sci Tech, 2022, 228: 109674

Acknowledgements This work was supported by the National Key R&D Program of China (2019YFA0706802), Shenzhen Science and Technology Program (CJGJZD20210408092602006), and the Science and Technology Major Project of Henan Province (221100240400).

Author contributions Yang D and Sun C conducted the experiments. Han Z, Yuan B, Chen J, and Pan D conducted the theoretical simulations and some experiments. Yang D, supervised by Xu H, Liu C, and Shen C, wrote and revised the manuscript. All authors contributed to the data analysis, discussed the results, and commented on the manuscript.

Conflict of interest The authors declare that they have no conflict of interest.

Supplementary information Experimental details and supporting data are available in the online version of the paper.

Dezhen Yang is currently a graduate student of Zhengzhou University, China. He received his Bachelor's degree in engineering from Chongqing University of Business and Technology, China in 2021. His current research interests focus on flexible strain hydrogel sensors.

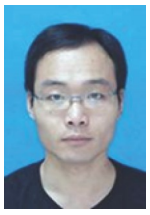

Huajie Xu is currently an associate professor of Zhengzhou University, China. He received his doctor's degree in engineering from the Northwestern Polytechnical University, China in 2015. His current research interests focus on composites, polymers and hydrogels.

分子间相互作用调控丝素蛋白/聚丙烯酰胺水凝胶的网络形貌和β片结晶，赋予水凝胶优异的黏附、应变和传感性能

杨德桢, 孙传强, 韩哲, 袁宝刚, 潘栋, 陈金传, 许华杰*, 刘春太, 申长雨

摘要 丝素蛋白(SF)作为一种特殊的天然聚合物，具有优异的生物相容性、生物降解性和双亲性，是制备柔性传感器的良好候选者. 然而，丝素蛋白的高结晶度和结晶不可控性使获得这种出色的仿生水凝胶传感器具有挑战性. 纯SF水凝胶是脆性的，没有黏性. 在此，我们通过引入聚丙烯酰胺(PAM)到SF水凝胶中来解决这一问题. 由于SF/PAM水凝胶具有较强的分子间相互作用，其网络形貌由欧几里得孔改变为非欧几里得孔. 同时，其β片结晶很容易被抑制到纳米尺度. 这些演变不仅使SF/PAM水凝胶具有优异的机械性能，而且具有出色的黏附性能. 与纯PAM水凝胶相比，SF8/PAM水凝胶的拉伸强度、拉伸破坏应变、抗压强度(80%应变下)和黏附性能(在猪皮上)分别提高了133.1%、120.9%、610.8%和104.8%. 此外, SF的双亲性可以使碳纳米管(CNTs)在水凝胶中分散良好. 制备的CNT0.3/SF8/PAM水凝胶继承并进一步改善了上述性能. 除此之外，它还表现出优异的自黏附传感性能，最大灵敏度因子高达10.13，工作应变范围超过1000%，大应变下稳定循环拉伸达500次以上. 同时，六种人类活动的精确检测也得到了验证. 本工作为实现高性能SF基水凝胶提供了新策略，并证实SF/PAM水凝胶在柔性可穿戴应变传感器中具有广阔的应用前景.

